Target Rediscovery on Long-wave Infrared Hyperspectral Images using Radiance and Emissivity Data

Alper Koz[a], İlke Belenoğlu[b], Mustafa Kütük[a], Seniha Esen Yüksel[b] and A. Aydın Alatan[a,c]
Center for Image Analysisa, Department of Electrical and Electronics Engineeringc, Middle East Technical University, Ankara, 06800.
Department of Electrical and Electronics Engineeringb, Hacettepe University, Ankara, 06800.
TURKEY

{koz, mkutuk, alatan}@metu.edu.tr, ilkebelenoglu@hacettepe.edu.tr, eyuksel@ee.hacettepe.edu.tr

ABSTRACT

Hyperspectral image target detection and rediscovery have until now mostly utilized visible near infrared (VNIR) and short wave infrared (SWIR) hyperspectral images. The target detection on the long wave infrared (LWIR) hyperspectral images on the other hand is barely studied, which is mainly due to the scarcity of the available LWIR data. This paper investigates the performance of different hyperspectral target detection methods for target rediscovery on LWIR hyperspectral images. The targets in the experiments are selected as the vehicles in the captured scenes at different times. The scope of the performed experiments includes the investigation and comparison of detection performances with respect to the radiance and emissivity data, with respect to the selected methodology where the detection is performed over individual pixels, group of pixels, and superpixels, and with respect to the utilized detection algorithm, which includes the representatives of four class of methods, namely spectral angle mapper (SAM), adaptive coherence estimator (ACE), orthogonal subspace detector (OSP), and hybrid structured detector (HSD). The experiments first indicate that the superiority of the detection performances for radiance and emissivity data does not indicate a significant change in thermal domain with respect to the vehicle colors. Second, using group of pixels for detection gives better results than using individual pixels. Superpixels on the other hand indicate the worst performance as the boundaries of the extracted superpixels are not very well aligned with the target boundaries. Finally, ACE algorithm reveals the best detection performance on LWIR images among the compared algorithms.

Keywords: *Long wave infrared, Hyperspectral Target Rediscovery, radiance, emissivity*

1. INTRODUCTION

Target detection with hyperspectral imaging (HSI) systems have until now found a huge number of applications in land cover mapping, mineral exploration, food quality, security, and forensics [1-4]. Most of these studies mainly utilize visible near infrared (VNIR) spectrum between 0.7 μm and 1 μm, and short wave infrared (SWIR) spectrum between 1 μm and 2.5 μm. Among these works, land cover mapping applications [5] have mainly utilized SWIR region, which includes the characteristics bands for water, vegetation and moisture detection. The surveillance studies for stand-off detection of explosives are mostly based on the reflectance characteristics of those materials in the range of 1.5 μm- 1.7 μm [6-7]. The researches on target rediscovery [8-9], which aims to find the position of a target in subsequent hyperspectral images, also perform detection and tracking by selecting and weighting certain wavelengths in SWIR range.

While hyperspectral target detection in VNIR and SWIR bands has reached to a good maturity, the related research in LWIR region can still be regarded as in its infancy stage, mostly due to the scarcity of data and the specific challenges in LWIR images such as the variations in temperatures and the noisy nature of the captured data. As one of the few target detection research in LWIR range, Blake et al [10] identify the materials with different emissivity by performing atmospheric compensation and temperature-emissivity

separation [11] and then utilizing adaptive coherence estimator (ACE) for detection. In a recent study of the same group [12], the performances of different target detection algorithms are compared with respect to the atmospheric compensation and target temperatures.

The aim of this paper is to investigate the performance of different methods for target rediscovery on hyperspectral LWIR images. The targets in the experiments are selected as the vehicles in the captured scenes. The scope of the performed experiments includes the investigation and comparison of target detection performances,

- with respect to the type of the data, namely, radiance and emissivity data,
- with respect to the selected methodology, where the target detection is performed over individual pixels, group of pixels, and superpixels,
- and with respect to the utilized target detection methods, which involve the representatives of four class of methods, namely, (i) spectral angle mapper (SAM), (ii) adaptive coherence estimator (ACE), (iii) orthogonal subspace detector (OSP), and (iv) hybrid structured detector (HSD).

The performance metrics for the comparisons are selected as the false positive rate and true positive rates. The results are given in terms of the false positive rates for the true positive rate of 100 %. The percentage of the test images, where the target is detected without any false positives, over all the images, is employed as a second performance metric.

The next section explains the main methodologies for target detection over radiance and emissivity data. Section 3 presents the experimental data set, which is followed by the experimental results and comparisons in Section 4. The conclusions are presented in Section 5.

2. PROPOSED METHODOLOGIES FOR TARGET REDISCOVERY

Figure 1 gives the general scheme for the target detection on hyperspectral LWIR images. Three different methodologies are considered for target detection, namely, matching over pixels, matching over group of pixels, and matching over superpixels. The performances of two different types of data, radiance and emissivity, are tested for the detection.

In the case of detection over pixel radiance, the radiance spectra of the image pixels directly go into the detection algorithm. The matching algorithm gives the similarity of the radiance spectra of each pixel with the reference spectra of the target. The resulting similarity score are then evaluated with respect to the false positive and true positive (recall) rates.

In the case of detection over group of pixels, which can be utilized for the targets larger than one pixels, the

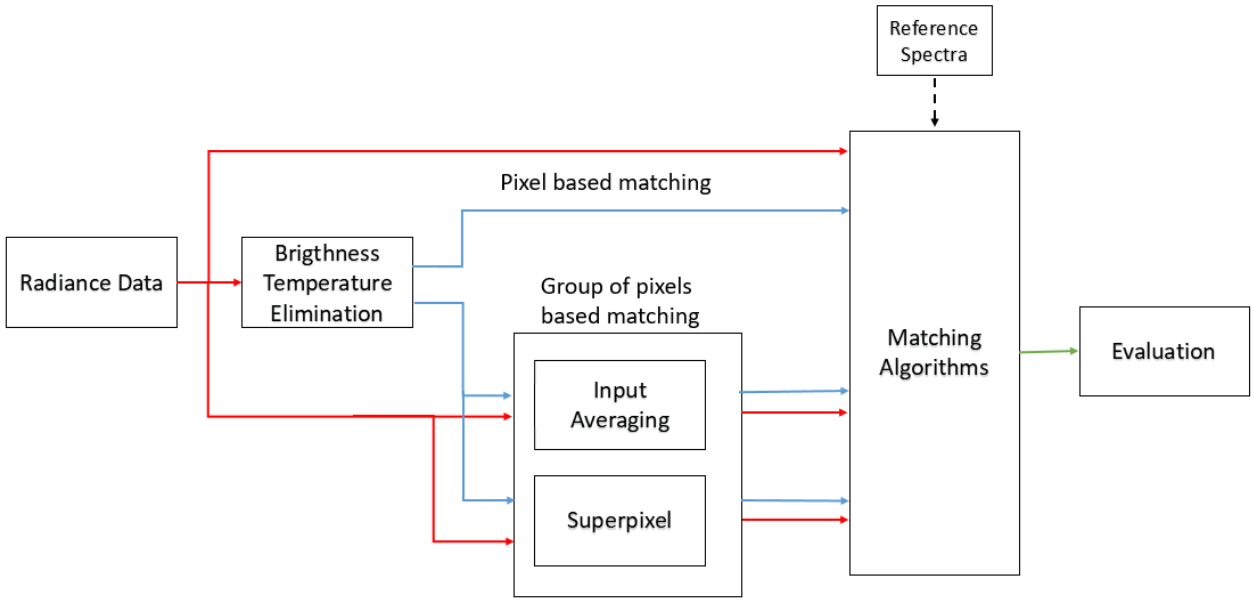

Figure 1: General scheme of the proposed target detection methods

spectral bands of the hyperspectral image are first passed through a spatial filter. This filter can be selected as an averaging filter or as a difference of averaging filters. Based on the initial experiments, the following difference of averaging filter is utilized for the tests:

$$h = \begin{bmatrix} 3 & 3 & 3 \\ 3 & 4 & 3 \\ 3 & 3 & 3 \end{bmatrix} \quad (1)$$

After the averaging operation, the hyperspectral image enters to the matching algorithm.

In the case of detection over superpixels, the hyperspectral image is divided into the superpixels considering the size of the searched targets. Then, the spectral mean of each superpixel is entered to the matching algorithm for detection.

The same approaches are also applied to the emissivity data as well. The emissivity of the pixels for the LWIR images is estimated by subtracting the thermal component in the radiance spectra of the images. The thermal component is approximated by minimizing the mean square error between the radiance spectrum and the Planck curves iteratively generated for the possible temperatures within a temperature range [13]. The Planck curve generated for the estimated brightness-temperature is substracted from the radiance spectra and inputted to the target detection algorithm. This difference can be regarded as an *approximation of emissivity* or *detailed component* of the radiance spectra involving the characteristical information about the pixel, which can be used for detection. However, the similar results are also obtained for the other TES algorithms as well [14].

3. HYPERSPECTRAL DATA SET

The hyperspectral images are captured with SEBASS sensor [11] from a height of 500 m. above ground level. The spectral range of the images is from 7.6 µm -13.5 µm involving 128 bands. Two sets of LWIR hyperspectral images are utilized for the experiments. The sample bands for each image are illustrated on

Figures 2 and 3, respectively, for both sets. Red, blue and magenta shows the three target vehicles 1, 2, and 3 respectively. Table 1 and 2 give the detailed information about their sizes, capturing times and target information. Overall, there are 5 images in the first set including three targets and 7 images in the second set including only one target. .

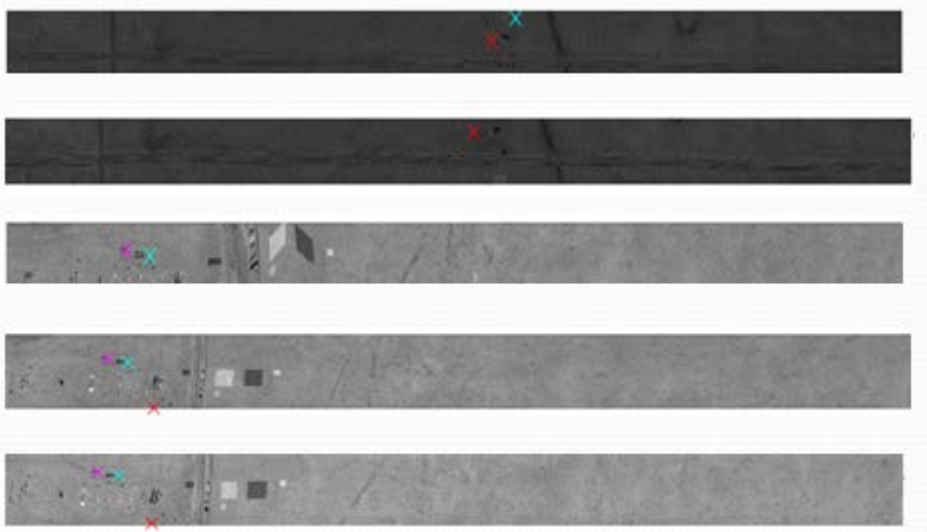

Figure 2: Sample bands from Experimental Data Set 1 and target positions

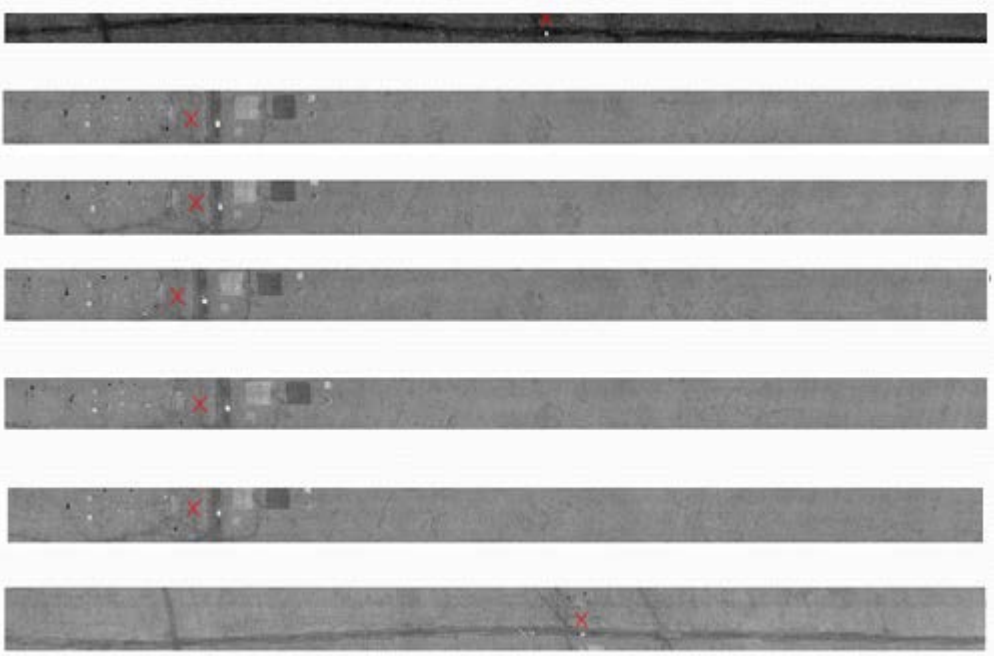

Figure 3: Sample bands from Experimental Data Set 2 and target positions

Table 1: Information regarding the first set of hyperspectral LWIR images and targets

Image	Image Size	Capture Date and Hour	Target No and Their Colors
1	2500 x 128	11/08/2014, 18:14	1 (black), 2 (white)
2	2500 x 128	11/08/2014, 18:40	1 (black)
3	1532 x 128	11/08/2014, 13:35	2 (white), 3 (black)
4	1531 x 128	11/08/2014, 18:19	1 (black), 2 (white), 3 (black)
5	1510 x 128	11/08/2014, 18:28	1 (black), 2 (white), 3 (black)

Table 2: Information regarding the second set of hyperspectral LWIR images and targets

Image	Image Size	Capture Date and Hour	Present Targets and Their Colors
1	5000 x 128	11/08/2014, 21:41	1 (black)
2	2937 x 128	11/08/2014, 21:50	1 (black)
3	2921 x 128	11/08/2014, 21:55	1 (black)
4	2924 x 128	11/08/2014, 22:00	1 (black)
5	2930 x 128	11/08/2014, 22:04	1 (black)
6	2912 x 128	11/08/2014, 22:09	1 (black)
7	2500 x 128	11/08/2014, 22:18	1 (black)

4. EXPERIMENTAL RESULTS AND DISCUSSIONS

This section presents the experimental results with respect to the radiance and emissivity data and their comparisons. As conventional precision-recall curves are not suitable for a regular comparison due to low number of target pixels, another metric based on false positive rates is utilized. For that purpose, the target's score is used as a threshold and the pixels whose scores are larger than this value are counted as false positives. In other words, the number of false positives is used as the performance metric when precision is 100 %. Nevertheless, relying solely on this metric can give confusing results when multiple images are used to compare algorithms, because some of the images can give a very high number of false positives that overwhelms the other results. To solve this issue, a second metric as the percentage of the test images where the target detection is achieved with zero false positives is utilized for the comparisons. The experiments conducted in the following sections are interpreted using these two metrics.

4.1 Target Detection Results for Radiance Data

In this experiment, the pixel spectra taken from the target position from each hyperspectral test image is

searched in other images in radiance domain. Both pixel and group of pixels based target detection are compared in those experiments. The superpixel based detection results are excluded from the comparisons as the segmentation with the superpixels does not provide successful performances in terms of boundary recall and segmentation error. The results for a sample run using ACE algorithm is given in the Table 3. In the table, rows represent the image, from which the reference signature of target is taken, while columns represent the test image, where the target is searched. Results are shown as false positive counts for each reference and test image pairs and their summation for the reference signatures. It should be noted that while the number of false positives are very low in most of the images, there is a huge number of false positives in some particular images. Therefore, these images unfairly dominate the overall false positive counts, which generate an unfair evaluation of the performances. As mentioned, this situation is tried to be avoided by defining a second performance metric in terms of the total number of pairs which give zero false positives.

Figure 4 illustrates a comparison of target detection approaches based on pixels and group of pixels. The reference signature from Image 4 is used in the given example. The pixel based approach gives false positive counts of 41, 20, 0, 0 and 2 for the 5 images illustrated in the figure. False positive locations are mostly other cars in the test site and placed targets into the experimental site like black vehicle paint and glass. In the case of group of pixel based approach, a significant decrease is observed in the number of false positives. For instance, the number of false positives is decreased from 41 to 28 for the first image, while the target is successfully detected without any false alarm for the other images. The spatial filtering in fact decreases the signal to noise ratio for a better performance in LWIR images.

Table 4 gives the total false positive rates for SAM, ACE, OSP, and HSD algorithms for both pixel and group of pixel based target detection on 2 different sets for 4 different targets. It can be seen that ACE algorithm gives the best results for LWIR radiance based target detection. One can conclude that group of pixel based approach gives higher false positive rates for the ACE algorithm. However, this is mainly due to the outlier images, which give a huge number of false positives as illustrated in Table 3. To avoid such confusion, Table 5 gives also the detection rates over all the pairs for the same algorithms and approaches in terms of the second performance metric. It can be concluded that even though group of pixels based approach increases the false positive counts, it significantly increases the total detection rate.

Table 3: Target detection results in radiance domain for target 1 in set 1, using ACE algorithm

Image No		*T1*	*T2*	*T3*	*T4*	*T5*	*Total*	*Rate (%)*
R1	**P**	0	0	10	0	0	10	0.001
	SF	0	139	1	0	0	140	0.011
R2	**P**	6	0	1	0	0	7	0.001
	SF	3	0	0	0	0	3	0.001
R3	**P**	24	1	0	5	2	31	0.002
	SF	2	0	0	0	0	2	0.001
R4	**P**	41	20	0	0	2	63	0.005
	SF	28	0	0	0	0	28	0.002
R5	**P**	28	13	11	0	0	52	0.004
	SF	64	21	13	0	0	98	0.008

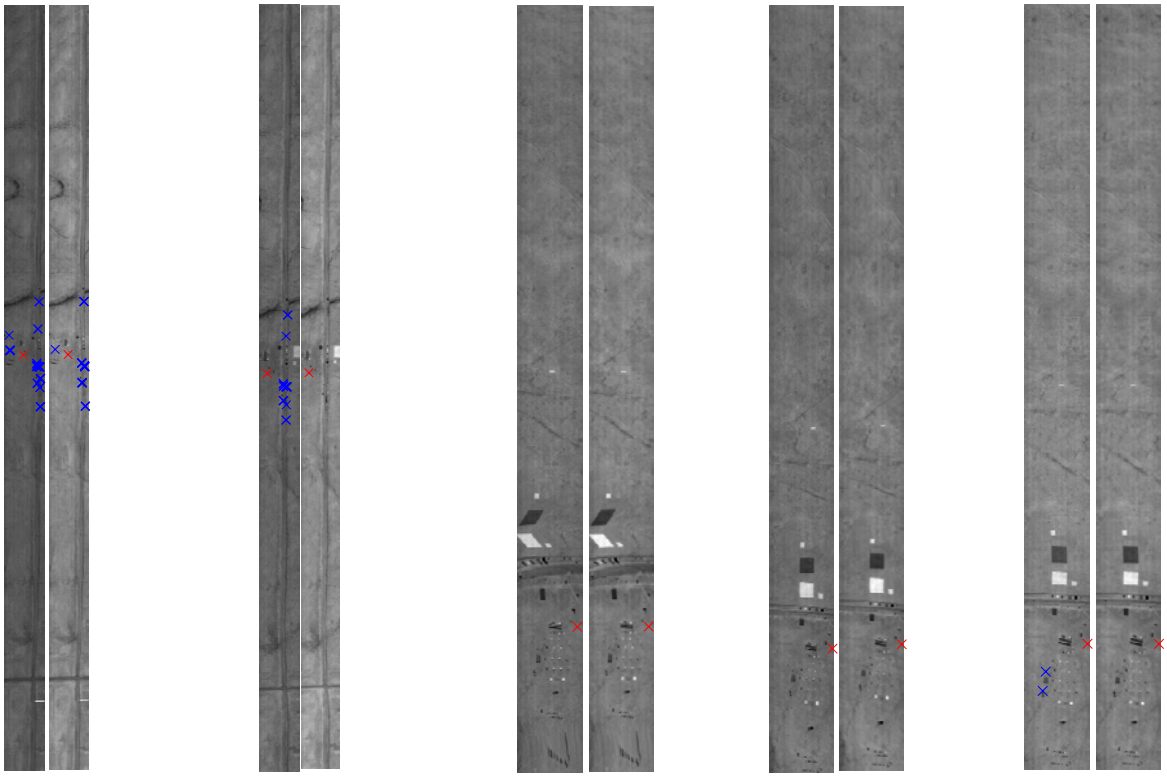

(a) (b) (c) (d) (e)

Figure 4: Pixel based (left) vs group of pixels based (right) target detection. Targets and false positives are illustrated with red and blue crosses, respectively. (a) Image 1, (b) Image 2, (c) Image 3, (d) Image 4, (e) Image 5.

Table 4: Total false positive rates using LWIR radiance data

	Matching Algorithm	Target 1 Set 1 (%)	Target 2 Set 1 (%)	Target 3 Set 1 (%)	Target 1 Set 2 (%)
Pixel Based	**SAM**	2.3652	0.0856	0.6310	0.0028
	ACE	0.0027	0.0009	0.0003	0.0013
	OSP	0.7340	0.0087	0.0003	0.0127
	HSD	1.3569	0.0004	0.0003	0.0001
Group of Pixels Based	**SAM**	12.0139	1.9467	0.1265	3.0756
	ACE	0.0044	0.0001	0.0002	0.0264
	OSP	6.1819	5.2492	0.0011	3.9974
	HSD	20.6007	8.9464	0.0010	0.0903

Table 5: Total detection rates using LWIR radiance data

	Matching Algorithm	Target 1, Set 1 (%)	Target 2, Set 1 (%)	Target 3 Set 1 (%)	Target 1 Set 2 (%)
Pixel Based	**SAM**	5	25	17	59
	ACE	35	83	67	43
	OSP	30	42	67	45
	HSD	15	75	50	79
Group of Pixels Based	**SAM**	10	25	67	69
	ACE	60	83	50	59
	OSP	10	8	50	50

	HSD	20	75	67	69

4.2 Target Detection Results for Emissivity Data

The same experiments in Section 4.1 are also repeated for emissivity data obtained from temperature emissivity separation. Table 6 gives the average detection rates over all pairs in percentage. It can be seen that ACE matching algorithm also gives the best results in emissivity domain. In addition, the group of pixel based approach also mostly gives better results with respect to the pixel-wise detection.

Table 6: Total detection rates using LWIR emisivity data

	Matching Algorithm	Target 1, Set 1 (%)	Target 2, Set 1 (%)	Target 3 Set 1 (%)	Target 1 Set 2 (%)
Pixel Based	**SAM**	5	17	17	55
	ACE	20	83	33	52
	OSP	30	58	33	57
	HSD	25	66	50	64
Group of Pixels Based	**SAM**	25	25	50	62
	ACE	60	75	83	67
	OSP	30	33	67	67
	HSD	20	37	67	69

4.3 Comparison of Target Detection with Radiance and Emissivity Data

In this section, the experimental results are separately compared for radiance and emissivity based detection for the case of ACE algorithm, which gives the best performance over all methods. Table 7 gives total detection rates for white (Target 2) and black (others) cars. From these results, it can be concluded that emissivity conversion does not affect the detection rate for the white car. On the other hand, it is also observed that it does not indicate a stable performance increase or decrease for the black cars as well.

Table 7: Radiance and emisivity comparisions based on total detection rates

Set ID	Target ID	Radiance	Emissivity
Set 1	**Target 1 (black)**	35 %	20 %
	Target 2 (white)	83 %	83 %
	Target 3 (black)	67 %	33 %
Set 2	**Target 1 (black)**	43 %	52 %

4. CONCLUSIONS

The experiments with different methodologies and algorithms on have revealed the following conclusions regarding the target detection on hyperspectral LWIR images. First, group of pixel based detection has indicated a significantly better result with respect to the pixel wise detection in the tests. However, the performance of the superpixel based approach was not satisfactory. The poor results for the superpixel based approach can be linked with the success of oversegmentation to track object boundaries in particular due to the comparatively noisy nature of thermal range hyperspectral images. Among the utilized algorithms, SAM, ACE, OSP and HSD, it has been observed that ACE have indicated the best performance for LWIR images. Regarding the type of the data, it can be concluded that emissivity conversion does not affect the detection rate for the white car. On the other hand, it does not indicate a stable performance increase or decrease for the black cars as well.

REFERENCES

[1] M. J. Khan, H. S. Khan, A. Yousaf, and A. Abbas, “Modern Trends in Hyperspectral Image Analysis: A Review”, IEEE Access, vol. 6, pp. 14118-14129, Mar. 2018

[2] P. Yuen and M. Richardson, “An introduction to hyperspectral imaging and its application for security, surveillance and target acquisition”, The Imaging Science Journal, vol. 58, no. 5, pp. 241-253, 2010.

[3] G. Camps-Valls, D. Tuia, L. Bruzzone, and J. A. Benediktsson. Advances in hyperspectral image classification: Earth monitoring with statistical learning methods. IEEE Signal Processing Magazine, vol. 31, no. 1, pp. 45-54, Jan. 2014

[4] H. Soydan, A. Koz, H. S. Düzgün, “Identification of hydrocarbon microseepage induced alterations with spectral target detection and unmixing algorithms”, Int. J. Applied Earth Observation and Geoinformation, vol. 74, pp. 209-221, Feb. 2019

[5] R. Hale, E. Sertel and N. Musaoğlu, “Assessment of Classification Accuracies of SENTINEL-2 and LANDSAT-8 Data for Land Cover/Use Mapping”, The International Archives of the Photogrammetry, July 2016.

[6] M. P. Nelson, A. Basta, R. Patil, O. Klueva, P. J. Treado, “Development of a handheld widefield hyperspectral imaging (HSI) sensor for standoff detection of explosive, chemical, and narcotic residues”, Next-Generation Spectroscopic Technologies VI, Proc. SPIE 8726, 2013.

[7] B. M. Onat, G. Carver, and M. Itzler, “A solid-state hyperspectral imager for real-time standoff explosives detection using shortwave infrared imaging,” Non-Intrusive Inspection Technologies II, Proc. SPIE 7310, 2009.

[8] J. Kerekes, M. Muldowney, K. Strackerjan, L. Smith, and B. Leahy. Vehicle tracking with multi-temporal hyperspectral imagery. In Defense and Security Symposium, pages 62330C–62330C. International Society for Optics and Photonics, 2006.

[9] B. Uzkent, A. Rangnekar, and M. Hoffman. Aerial vehicle tracking by adaptive fusion of hyperspectral likelihood maps. The IEEE Conference on Computer Vision and Pat- tern Recognition Workshops (CVPRW), July 2017.

[10] Blake M. Rankin, Joseph Meola, and Michael T. Eismann, "Spectral Radiance Modeling and Bayesian Model Averaging for Longwave Infrared Hyperspectral Imagery and Subpixel Target Identification" IEEE Trans. Geosci. Remote Sensing, vol. 55, no. 12, 2016.

[11] C. C. Borel, “Surface emissivity and temperature retrieval for a hyperspectral sensor,” presented at the Int. Geosci. Remote Sens. Symp. Sens. Manag. Environ., 1998.

[12] Nathan P. Wurst, Seung Hwan An, Joseph Meola, “Comparison of longwave infrared hyperspectral target detection methods”, Proc. SPIE 10986, Algorithms, Technologies, and Applications for Multispectral and Hyperspectral Imagery XXV, 1098617, May 2019.

[13] A Koz, A. Çalışkan, and A. Aydın Alatan, “Registration of MWIR-LWIR Band Hyperspectral Images”, in Proc. of 8th Workshop on Hyperspectral Image and Signal Processing: Evolution in Remote Sensing, Los Angeles, USA, 2016.

[14] Alan Gillespie, Shuichi Rokugawa, Tsuneo Matsunaga, J. Steven Cothern, Simon Hook, and Anne B.

Kahle, “Temperature and Emissivity Separation Algorithm for Advanced Spaceborne Thermal Emission and Reflection Radiometer (ASTER) Images”, in IEEE Transactions on Geoscience and Remote Sensing, pp. 1113-1126, Vol. 36, No. 4, July 1998.